AMERICAN SOCIETY FOR MICROBIOLOGY | Applied and Environmental Microbiology®

ENVIRONMENTAL MICROBIOLOGY

Impact of River Channel Lateral Migration on Microbial Communities across a Discontinuous Permafrost Floodplain

Madison M. Douglas,[a] Usha F. Lingappa,[a] Michael P. Lamb,[a] Joel C. Rowland,[b] A. Joshua West,[c] Gen Li,[a] Preston C. Kemeny,[a] Austin J. Chadwick,[a] Anastasia Piliouras,[b] Jon Schwenk,[b] Woodward W. Fischer[a]

[a]Division of Geological and Planetary Sciences, California Institute of Technology, Pasadena, California, USA
[b]Earth and Environmental Sciences Division, Los Alamos National Laboratory, Los Alamos, New Mexico, USA
[c]Department of Earth Sciences, University of Southern California, Los Angeles, California, USA

ABSTRACT Permafrost soils store approximately twice the amount of carbon currently present in Earth's atmosphere and are acutely impacted by climate change due to the polar amplification of increasing global temperature. Many organic-rich permafrost sediments are located on large river floodplains, where river channel migration periodically erodes and redeposits the upper tens of meters of sediment. Channel migration exerts a first-order control on the geographic distribution of permafrost and floodplain stratigraphy and thus may affect microbial habitats. To examine how river channel migration in discontinuous permafrost environments affects microbial community composition, we used amplicon sequencing of the 16S rRNA gene on sediment samples from floodplain cores and exposed riverbanks along the Koyukuk River, a large tributary of the Yukon River in west-central Alaska. Microbial communities are sensitive to permafrost thaw: communities found in deep samples thawed by the river closely resembled near-surface active-layer communities in nonmetric multidimensional scaling analyses but did not resemble floodplain permafrost communities at the same depth. Microbial communities also displayed lower diversity and evenness in permafrost than in both the active layer and permafrost-free point bars recently deposited by river channel migration. Taxonomic assignments based on 16S and quantitative PCR for the methyl coenzyme M reductase functional gene demonstrated that methanogens and methanotrophs are abundant in older permafrost-bearing deposits but not in younger, nonpermafrost point bar deposits. The results suggested that river migration, which regulates the distribution of permafrost, also modulates the distribution of microbes potentially capable of producing and consuming methane on the Koyukuk River floodplain.

IMPORTANCE Arctic lowlands contain large quantities of soil organic carbon that is currently sequestered in permafrost. With rising temperatures, permafrost thaw may allow this carbon to be consumed by microbial communities and released to the atmosphere as carbon dioxide or methane. We used gene sequencing to determine the microbial communities present in the floodplain of a river running through discontinuous permafrost. We found that the river's lateral movement across its floodplain influences the occurrence of certain microbial communities—in particular, methane-cycling microbes were present on the older, permafrost-bearing eroding riverbank but absent on the newly deposited river bars. Riverbank sediment had microbial communities more similar to those of the floodplain active-layer samples than permafrost samples from the same depth. Therefore, spatial patterns of river migration influence the distribution of microbial taxa relevant to the warming Arctic climate.

KEYWORDS permafrost, active layer, methanogenesis, methanotrophy, Koyukuk, Alaska

Citation Douglas MM, Lingappa UF, Lamb MP, Rowland JC, West AJ, Li G, Kemeny PC, Chadwick AJ, Piliouras A, Schwenk J, Fischer WW. 2021. Impact of river channel lateral migration on microbial communities across a discontinuous permafrost floodplain. Appl Environ Microbiol 87:e01339-21. https://doi.org/10.1128/AEM.01339-21.

Editor Isaac Cann, University of Illinois at Urbana-Champaign

Address correspondence to Madison M. Douglas, mmdougla@caltech.edu.

Received 7 July 2021
Accepted 26 July 2021
Accepted manuscript posted online 4 August 2021
Published 28 September 2021

Permafrost environments cover 24% of land area in the Northern Hemisphere and contain significant amounts of organic carbon in soil and sedimentary deposits (1, 2). This organic carbon (OC) has been largely isolated from microbial consumption, in some cases for thousands of years, due to low subsurface temperatures and ice-cemented sediment pore spaces (3). Currently, polar amplification of increases in global air temperature is causing rapid permafrost thaw that exposes previously sequestered organic carbon stores to greater rates of microbial degradation (4). The upper "active layer" of Arctic soils thaws each summer, in contrast to underlying permafrost, i.e., ground that has remained below 0°C for at least 2 years. As the active layer deepens interannually across the Arctic due to higher temperatures, labile OC becomes available for respiration by permafrost microbial communities, and active-layer microbes may penetrate deeper soil horizons. This soil carbon reservoir can be released to the atmosphere as methane (CH_4) or carbon dioxide (CO_2) or remain sequestered in Arctic sediments, depending on the affinities and activities of microbes present in permafrost environments (5).

Predicting microbial responses to permafrost thaw requires understanding changes in soil microbiomes with warming over decadal timescales within heterogeneous landscapes. Most understanding of permafrost microbial activity comes from laboratory incubation studies simulating deepening of the active layer. Previous work documented an initial spike in CO_2 emissions in the days following permafrost thaw, with peak CH_4 emissions occurring years after thaw (5–7). However, incubation studies range widely in their predictions of CO_2-C equivalent emissions, primarily due to challenges in mapping results from laboratory incubations to the three-dimensional structure of landscapes (6, 8). Furthermore, understanding the vertical structure of permafrost microbiomes requires time-integrated tracking of the depths of the active layer, water table, and seasonal frost, all of which may generate vertical discontinuities in microbial community composition (9, 10).

In addition to vertical variations in soil structure and microbial community, permafrost landscapes are laterally heterogeneous (11). Previous work correlating microbiome and landform heterogeneity focused on variations in soil saturation of ice wedge polygons near Barrow, AK (12), and in Stordalen Mire, Sweden (13–16). However, many organic-matter-rich permafrost deposits are located in the floodplains of large rivers, where fluvial processes control the transport of carbon and sediment and the resulting architecture of the deposits (17–19). In particular, river channel migration may introduce additional variability to the permafrost soil microbiome by eroding the active layer and upper tens of meters of underlying permafrost and by building new deposits elsewhere on the floodplain (20).

Arctic rivers can migrate laterally by meters per year (21), and river migration controls spatial patterns of grain size, surface water in lakes, and deposit age across floodplains (22). Meandering streams erode previous river channel deposits on the outside of bends in their sinuous channel paths, forming a steep cutbank (Fig. 1E). In locations with permafrost, the river must first thaw its cutbanks before being able to erode the thawed sediment (23). Most bank thaw and erosion occur during the spring snowmelt flood following ice breakup, which removes unconsolidated sediment and exposes permafrost to thawing by the river (24). At the same time that cutbanks are eroding, the river deposits sediment on the inside of bends, forming shallowly sloping point bars and maintaining a roughly constant channel width (Fig. 1C to E). These erosion and depositional processes gradually increase curvature until the channel eventually cuts itself off and subsequently begins the process anew. Point bar deposits display systematic, predictable trends in grain size: coarser sand or gravel occurs at depth, reflecting the size of sediment transported along the bed of the river, while deposits closer to the surface of the floodplain contain fine sand, silt and clay transported in the upper portion of the river water column (25).

In this study, we examined microbial community variation throughout various floodplain deposits of the Koyukuk River—a major tributary of the Yukon River that runs

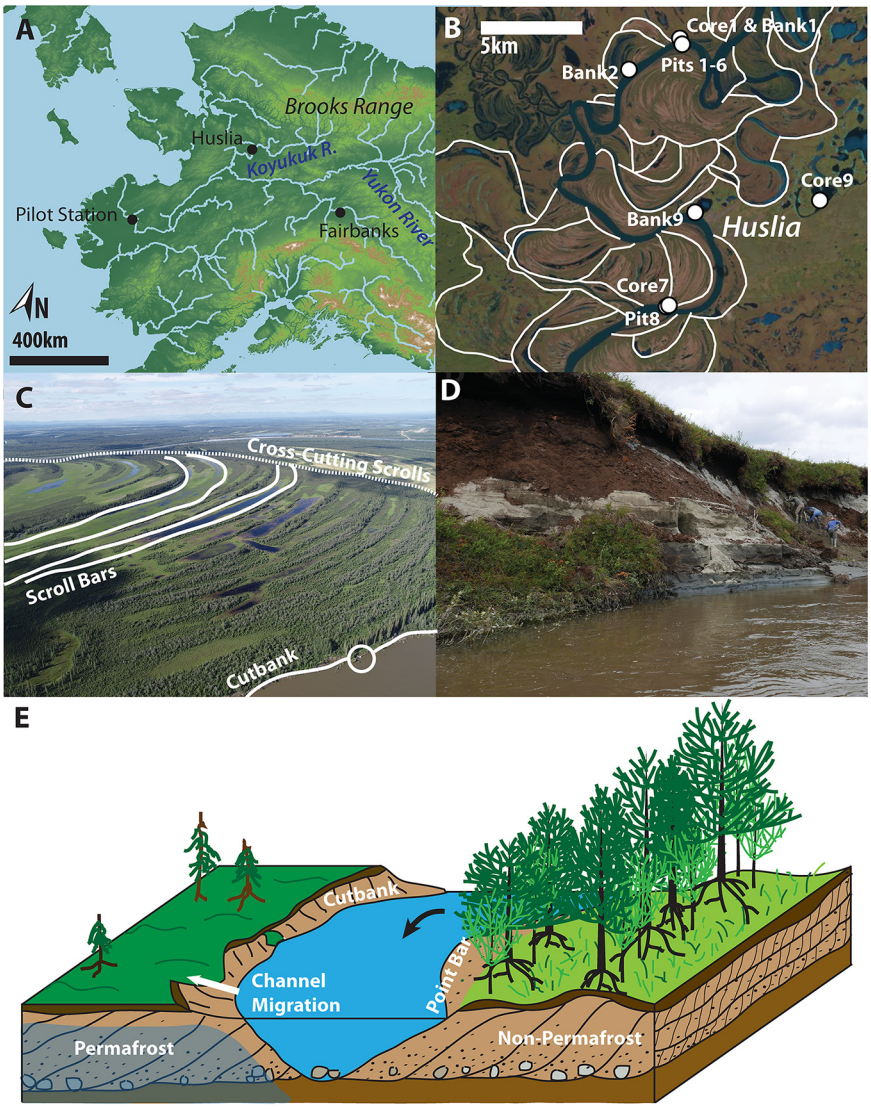

FIG 1 (A) Map of Alaska, with the study location near the village of Huslia on the Koyukuk River, a major tributary of the Yukon River. Base map generated in QGIS 3.4 using USGS GTOPO30 30 arc-second digital elevation model (68) and the HydroSHEDS 15 arc-second Arctic regional river shapefile (69) projected in WGS 84/NSIDC Sea Ice Polar Stereographic North. (B) Satellite imagery of the Koyukuk Flats floodplain marked with sampling locations and contacts between scroll bar complexes that illustrate cross-cutting relationships indicating their relative age. Core 1 was sampled approximately 10 m from the river cutbank, while bank 1 was sampled at the cutbank. Note the abundant scroll bar complexes that trace out past locations of the river channel as it migrated across the floodplain. (C) Oblique UAV photograph taken at 243 m above ground level of a meander bend on the Koyukuk River, with the boat circled for scale and water flowing away from the viewer. Unfrozen sediment is deposited on the sandy point bar and then becomes vegetated in alternating grass lake troughs and elevated, forested scrolls. (D) Field photo of permafrost river cutbank at sampling location bank 9, with undercut peat deposits over permafrost and a thick apron of thawed sediment containing slump blocks armoring the bank. (E) Schematic of river channel migration, with the river eroding an outer cutbank composed of former point bar deposits while depositing new sediment on the point bar on the right. The river flows out of the page (flow direction shown by black arrow), constructing cross-bedded strata in the point bar deposits that are coarser at the base of the channel and fine upwards. The river is migrating to the left (white arrow), eroding permafrost deposits (with permafrost shaded in blue and the active layer near the surface on the floodplain and the channel bank) with peat and black spruce vegetation, while the point bar consists of scrolls with ridges containing white spruce and deciduous trees alternating with troughs containing grasses.

through a floodplain underlain by discontinuous permafrost (Fig. 1A). The river is thawing and eroding permafrost along cutbanks exposed at the outside of its bends and depositing sediment on its inner bends without permafrost, generating a juxtaposition of permafrost, active-layer (including laterally thawed sediment on the riverbanks), and nonpermafrost environments with the same local climate (Fig. 1E, with scroll bars highlighted and direction of river migration indicated). Here, we compared the microbial community compositions of sediments from different landforms across the river floodplain to see if newly built, unfrozen point bar deposits contained a microbial community similar to that of their opposing, eroding permafrost cutbanks (Fig. 1B).

RESULTS

Microbial community diversity. Comparison of amplicon sequences to reference taxa indicated that members of the *Acidobacteria*, *Actinobacteria*, and *Proteobacteria* (mainly *Alphaproteobacteria* and *Betaproteobacteria*) were the most dominant phyla, followed by *Bacteriodetes*, *Chloroflexi*, and *Firmicutes* (Fig. 2). This is taxonomically consistent with previous studies of permafrost microbial communities (3, 12, 32).

A distinction between permafrost versus active-layer and nonpermafrost deposits was reflected in certain taxonomic groups. The families *Caldisericaceae*, vadinHA17 (*Bacteroidetes*), and *Clostridiaceae 1* are relatively abundant in our permafrost samples, while few representatives are present in nonpermafrost or active-layer samples (Fig. 3). Other groups, such as *Rhizobiales*, *Planctomycetaceae*, and *Gemmatimonadaceae*, displayed the opposite trend and were more abundant in nonpermafrost deposits (Fig. 3). Few groups exhibited consistent trends with depth, likely due to discontinuities in soil conditions at the base of the active layer (for permafrost samples) or at the depth of annual frost formation in nonpermafrost samples (12). Both permafrost and nonpermafrost samples contained *Anaerolineaceae*, while *Syntrophaceae* were more abundant in active-layer and permafrost deposits (Fig. 3) (33, 34). These taxa were classified into families associated with anaerobic taxa, including obligate anaerobes, suggesting that while anoxic conditions were common across the floodplain, there were potentially more reducing conditions in permafrost. Archaea typically accounted for $<$1% of sequence reads in nonpermafrost deposits (Fig. 2). In permafrost, several of our subsurface samples from below the active layer contained more than 10% of reads belonging to the *Archaea*. Archaeal abundance was driven by members of the *Euryarchaeota*, which made up a mean of 85% of archaeal reads in permafrost, 88% in the active layer, and 68% in nonpermafrost deposits. The remaining archaeal operational taxonomic units (OTUs) consisted of unclassified *Thaumarchaeota*, particularly "*Candidatus* Nitrosoarchaeum." Previous studies of ice wedge polygons found that autotrophic ammonia oxidizers from the *Nitrososphaerales* dominate the *Thaumarchaeota* found in permafrost, implying that *Archaea* may play an important role in nitrogen cycling in permafrost environments (35). Fewer than 1% of archaeal reads consisted of *Crenarchaeota* or other phyla (e.g., Asgard taxa).

Replicate sample splits analyzed from Core9-44-46 and Core9-109-115 generated highly similar relative OTU abundances (Fig. 4), which we quantified as the standard deviation of relative abundance for the most abundant listed taxa at the phylum and family level. In comparison to Core9-44-46-R1 and -R3, Core9-44-46-R2 displayed slightly higher *Acidobacteria* and *Chloroflexi* relative abundances and smaller amounts of *Euryarchaeota*, *Actinobacteria*, and *Alphaproteobacteria*. The differences in relative abundance contributed to the higher uncertainty in reads for Core9-44-46 (2.0% at the phylum level and 1.4% at the family level) versus Core9-109-115 (0.50% at the phylum level and 0.44% at the family level). However, the similar and consistent OTU occurrence and relative abundance between replicates indicates relatively low uncertainty due to potential sample contamination as well as DNA extraction, amplification, and sequencing.

We observed lower microbial diversity in permafrost than in active-layer samples and the highest diversity and evenness in nonpermafrost samples (Table 1; Fig. 5). We rarefied

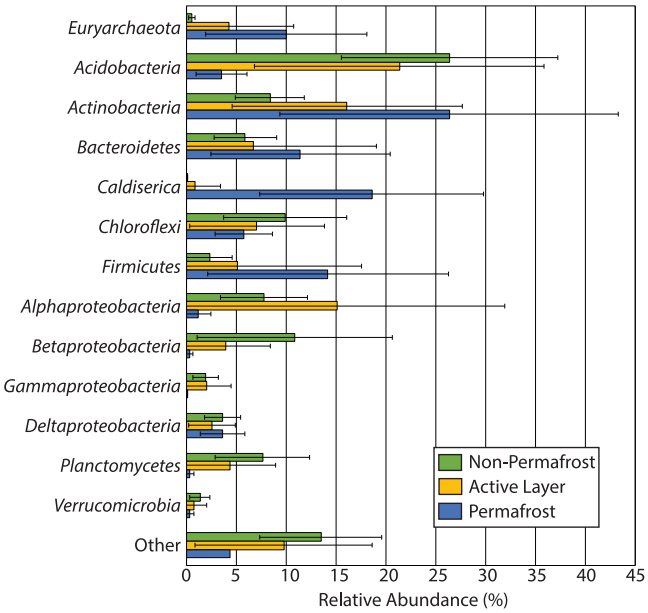

FIG 2 Mean relative taxon abundances for permafrost, active-layer, and nonpermafrost samples, with error bars showing the standard deviations of relative abundance within each grouping. The permafrost samples contained ice cement ($n = 8$: Core1-105-111 and core 9 samples > 58-cm depth), active-layer samples overlay ice cement ($n = 6$: core 1 and core 9 samples > 58-cm depth) or located on riverbanks with ice cement ($n = 8$: banks 1, 2, and 9), and nonpermafrost scroll bars were unfrozen ($n = 9$: core 7, pit 1, pit 2, pit 5, pit 6, and pit 8).

the data to 4,500 reads and did not conduct diversity analyses on samples with fewer reads out of concern that low reads were due to an error in sequencing and the data are not representative of the sample. However, we note that rarefying to 1,000 reads did not significantly change our results. The number of observed OTUs and the Shannon diversity index, Chao 1, Fisher's alpha, Simpson's evenness, and Simpson's index all indicated decreased diversity when transitioning from nonpermafrost to active-layer and permafrost samples. Active-layer samples from the floodplain cores and cutbanks showed similar diversity and evenness: floodplain active-layer samples had a Fisher's alpha of 1,272 ± 703 (mean ± 1 standard deviation) and a Simpson's evenness of 0.1254 ± 0.0830, while cutbank active-layer samples had a Fisher's alpha of 1,552 ± 1,106 and a Simpson's evenness of 0.1423 ± 0.1912 (Table 1). The floodplain and cutbank active-layer samples differed by <3% of the mean value of all other diversity metrics and had intermediate diversity between permafrost and nonpermafrost samples. Therefore, we inferred that the regions of the Koyukuk River floodplain that contain no permafrost hosted a greater variety of taxa. In contrast, permafrost and active-layer sediment contained microbial communities dominated by fewer taxa (Table 1; Fig. 5).

Nonmetric multidimensional scaling (NMDS) analyses of the microbial community data found distinct differences between the microbial communities of permafrost, active-layer, and nonpermafrost deposits, with active-layer samples spanning the space between isolated clusters of permafrost and nonpermafrost samples (Fig. 6A). Plotting the vectors of the most significant *de novo* taxa showed that most were from *Gemmatimonadaceae*, *Xanthobacteraceae*, *Syntrophaceae* (genus *Smithella*), and *Acidobacteria* subgroup 6. Some taxa commonly associated with nitrogen cycling, in particular *Bradyrhizobiaceae* and *Nitrosomonadaceae*, were highly significant and preferentially associated with nonpermafrost and active-layer deposits. We focused further analyses on the differences between permafrost, active-layer and nonpermafrost deposits in sequences assigned to families of biogeochemical interest but noted that large contributions to these differences come from sequences assigned to uncultured families and *Acidobacteria* subgroup 6.

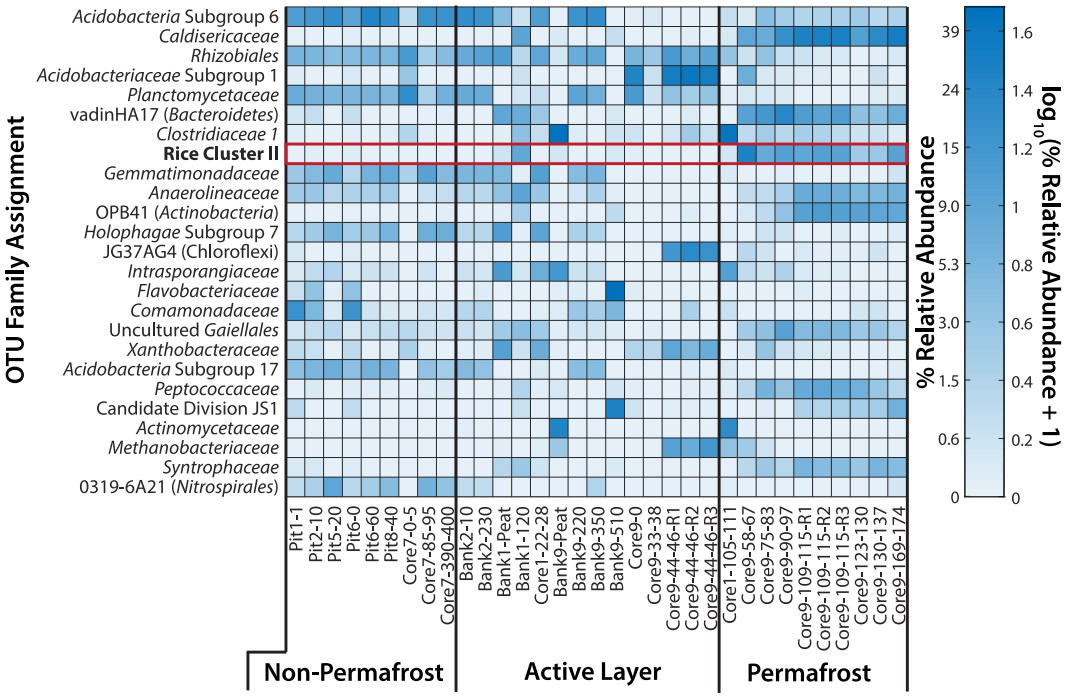

FIG 3 Heat map of dominant families in each sample. Note that members of the methanogenic Rice Cluster II (outlined in red) were abundant in permafrost and rare in nonpermafrost deposits. Sample core, pit, or bank number and depth in centimeters are indicated in sample names, and replicates are indicated as R1, R2 and R3. Nonpermafrost samples come from all depths in locations without observed permafrost, active-layer samples come from the zone of seasonal thaw on river banks or sediment overlying permafrost, and permafrost samples contained ice cement. Samples moving from left to right trend from more recent (nonpermafrost) river deposits to the oldest permafrost floodplain, and the samples at each location are listed moving from shallow to deep.

Taxa involved in methane biogeochemistry. Community analyses revealed that relative abundances of both methanogens and methanotrophs decrease upon permafrost thaw over seasonal timescales (Fig. 3). The main methanogenic taxa in our data belong to Rice Cluster II, which contains "*Candidatus* Methanoflorens stordalenmirensis" (100% similarity to IonTorrent metagenome SRA096214 using BLASTn)—a hydrogenotrophic methanogen whose abundance strongly correlated with soil methane concentrations in Stordalen Mire, Sweden (14, 16). OTUs assigned to Rice Cluster II were abundant in permafrost samples in this study, including those from core 1, bank 1, and core 9, accounting for up to 28.0% of reads (Fig. 3). We also observed less abundant taxa from the hydrogenotrophic genus *Methanobacterium* (up to 13.7% of reads) and the acetoclastic methanogenic genera *Methanosaeta* (up to 0.5% of reads) and *Methanosarcina* (up to 0.3% of reads) in core 9, core 1, bank 1, bank 9, and pits 1 to 8. In cutbanks that had been thawed by river migration, methanogen abundance was near or below the limit of detection (Fig. 7). Previous studies found similar trends with the hydrogenotrophic methanogens *Methanobacterium* and *Methanocellales* as well as the acetoclastic methanogens *Methanosarcina* and *Methanosaeta* (10, 15).

The main methanotrophic taxa in our data belong to GoM Arc I, which contains "*Candidatus* Methanoperedens nitroreducens," a species of ANME 2d. These are anaerobic methanotrophic (ANME) archaea that in cultured strains have a metabolism coupling methane oxidation to nitrate/nitrite reduction (37). OTUs assigned to GoM Arc I were abundant in one sample, Bank1-120, where they made up 10.9% of reads. ANME 2d archaea have been previously detected in permafrost microbial communities (38), often located in soil horizons slightly above horizons rich in methanogens (39). However, locations with abundant methanogens often contained few ANME archaea (e.g., core 9, $<$0.2% ANME relative abundance), while bank 1 contained a high relative abundance of ANME archaea but a low relative abundance of methanogens.

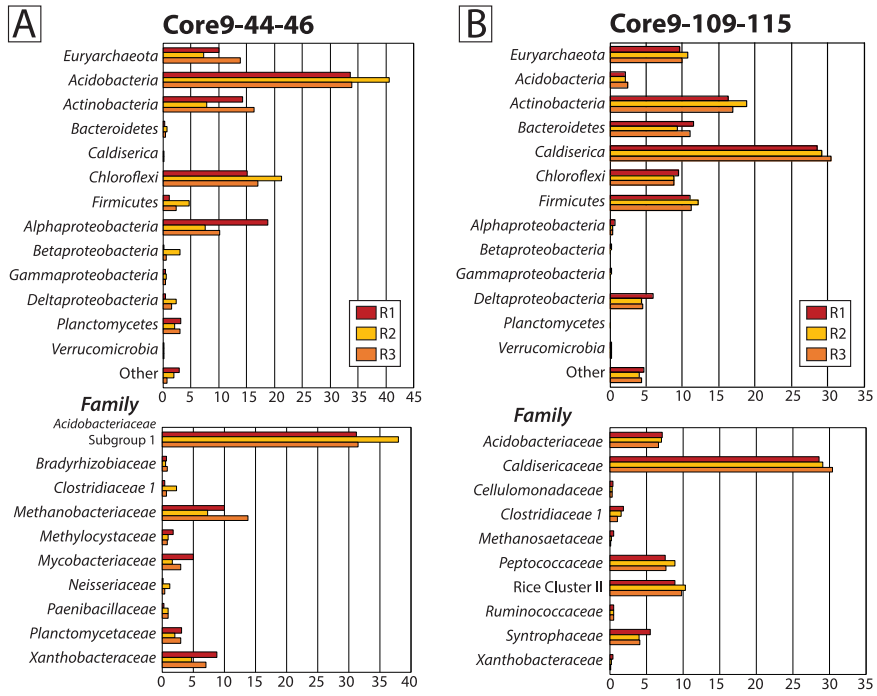

FIG 4 Comparison of replicate samples analyzed from (A) Core9-44-46 and (B) Core9-109-115 at the phylum and family taxonomic levels, displaying the 10 most abundant families for each sample.

We observed rare reads of potential aerobic methanotrophs in both permafrost and nonpermafrost deposits, classified as members of the alphaproteobacterial families *Methylocystaceae* and *Methylobacteriaceae*, the betaproteobacterial family *Methylophilaceae*, and the gammaproteobacterial families *Crenotrichaceae and Methylococcaceae* (see Table S1 in the supplemental material). However, these taxa were very low in abundance (taken together, 2.5% of reads in Core1-105-111 and $<$1% of reads in other samples) and therefore are likely to be minor contributors to methane consumption.

As a complementary approach to corroborate the presence of methanogenic and anaerobic methanotrophic taxa, we conducted qPCR analyses to examine the abundance of the methyl-coenzyme M reductase a-subunit functional gene (*mcrA*). Samples with abundant *Methanomicrobia* 16S amplicons (largely Rice Cluster II with minor contributions from other methanogenic taxa and GoM Arc I) also contained high abundances of the *mcrA* functional gene by qPCR (Fig. 8A), with the relative abundance of *mcrA* following trends with depth similar to those of the relative abundance of *Methanomicrobia* OTUs (Fig. 8B). Some samples (Core9-0, Core9-33-38, and Core9-44-46-R3) showed delayed amplification of *mcrA* (indicating the rare presence of the gene) but contained few or no amplicons attributed to known methanogenic or anaerobic methanotrophic taxa. We interpreted this to mean that these samples contained a very low abundance of such taxa ($<$0.001 relative abundance) whose presence was revealed by qPCR amplification. The samples with the highest *mcrA* gene abundances of samples with low or no methane-cycling taxa identified by 16S overlay sediment that both *mcrA* and 16S analyses indicated contains abundant *Methanomicrobia*, with the exception of Core7-85-95. Therefore, while qPCR results suggested that microbes carrying the *mcrA* gene may in fact be present in these samples at very low abundance, overall *mcrA* qPCR results lend support to metabolic inferences based on taxonomic classification of methanogen prevalence between sampling sites across the landscape (Fig. 8B).

We note that complete characterization of methane cycling on the Koyukuk floodplain requires constraining the activity, and not just the presence, of methanogens and methanotrophs (40). Previous work found that methanogenesis pathways inferred from 16S sequencing correlated with methane fluxes and δ^{13}C measurements made in

TABLE 1 Diversity metrics for the 16S amplification data, rarefied to 4,500 reads

Sample	No. of observed OTUs	Shannon diversity index	Chao 1	Fisher's alpha	Simpson's index	Simpson's evenness
Nonpermafrost						
Pit2-10	2,686	11.129	3,579	2,808	0.9992	0.4874
Pit5-20	2,720	11.006	4,894	2,910	0.9991	0.4050
Pit6-60	2,552	10.599	5,820	2,444	0.9964	0.1093
Pit8-40	2,777	11.018	6,275	3,090	0.9991	0.4158
Core7-0-5	2,099	10.239	3,102	1,531	0.9973	0.1739
Core7-85-95	1,573	8.960	3,178	859	0.9795	0.0310
Core7-390-400	1,032	8.505	1,848	419	0.9932	0.1421
Active layer						
Bank2-10	2,977	11.260	5,887	3,835	0.9994	0.5849
Bank2-230	2,157	9.989	4,619	1,626	0.9900	0.0461
Bank9-Peat	877	6.225	1,901	325	0.9122	0.0130
Bank9-220	1,656	9.662	3,646	946	0.9939	0.0989
Bank9-350	2,215	9.141	4,477	1,727	0.9569	0.0105
Bank9-510	1,010	7.469	1,955	405	0.9686	0.0316
Bank1-Peat	2,171	10.277	3,422	1,650	0.9973	0.1683
Bank1-120	2,308	10.209	7,344	1,901	0.9977	0.1850
Core1-22-28	2,352	10.529	3,894	1,989	0.9981	0.2201
Core9-33-38	1,759	9.055	5,969	1,063	0.9938	0.0913
Core9-44-46-R1	1,474	8.807	2,965	763	0.9895	0.0648
Permafrost						
Core1-105-111	678	5.606	1,674	222	0.9016	0.0150
Core9-58-67	1,099	7.470	1,722	464	0.9410	0.0154
Core9-90-97	2,059	9.466	5,570	1,468	0.9915	0.0573
Core9-109-115-R2	1,268	7.596	3,417	587	0.9631	0.0214
Core9-169-174	1,364	7.786	3,892	666	0.9724	0.0265

permafrost at Stordalen Mire (14). Our findings indicated that concentrations of methanogen and methanotroph DNA detectable via 16S sequencing and correlated abundance of the *mcrA* functional gene—a minimum constraint for methane production and consumption—were found only in permafrost terrain far from the river channel. Improved understanding of covariance of landscapes with microbial communities can guide further analysis—such as field- and laboratory-based measurements and incubations to measure methane flux—required to further characterize and quantify methanogen and methanotroph activity (41).

Soil geochemistry. To evaluate how sediment properties might influence microbial diversity, we conducted scaled principal-component analysis (sPCA) on our diversity metrics and metadata, including OC content, stable isotope ratios, sample depth, and median grain size (Tables 2 and 3). The first two sPCA components accounted for 47% and 19% of the variance in community composition, respectively. Our results show that the first component depended primarily on diversity indices (observed OTUs, Chao 1, Simpson's evenness, Fisher's alpha, Shannon index, and Simpson's index) and sample classification as permafrost, active layer, or nonpermafrost (Fig. 5). The second component is mainly dependent on total organic carbon (TOC), total nitrogen (TN), and the TOC/TN ratio, with secondary contributions for sample depth and median grain size (Fig. 6B). Many of these variables are highly correlated; we observed higher TOC and TN contents in finer-grained sediment, similar to previous studies on sediments from other Arctic rivers (42, 43). In turn, point bar deposits tended to be finer grained closer to the floodplain surface (25), so TOC content was also weakly anticorrelated with sample depth. However, sample classification as permafrost, active layer, or nonpermafrost appeared to dominate variations in sediment geochemistry in determining taxa presence and diversity (Fig. 5). We also noted that in our study area, vegetation varies with permafrost occurrence (26), so the changes in microbial community between frozen and unfrozen sediment may also be a result of different ecological niches available in the permafrost and nonpermafrost rhizospheres (44).

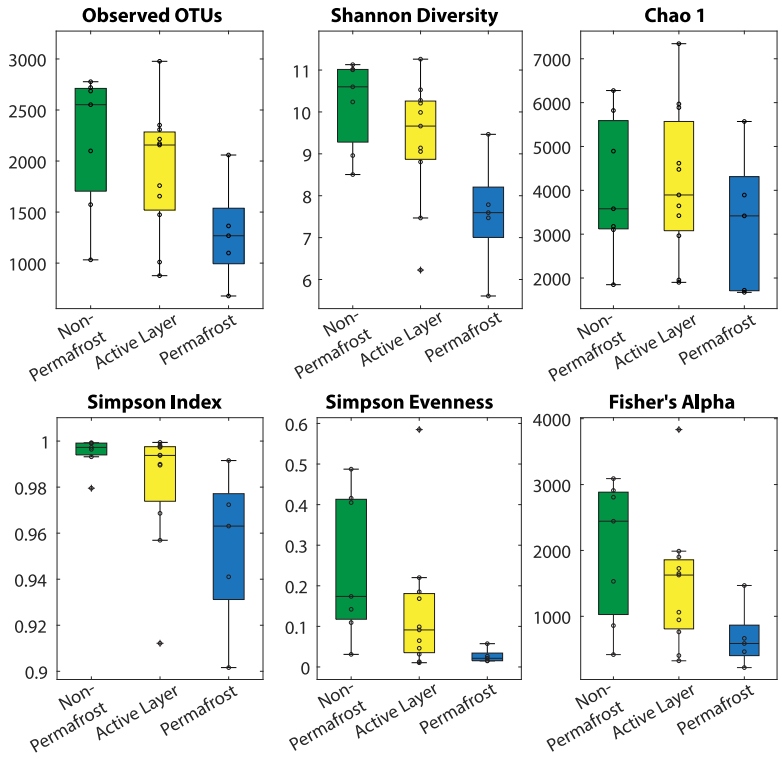

FIG 5 Box-and-whisker plots indicating the median and the 25th and 75th percentiles of diversity index distributions. Samples are grouped as nonpermafrost (no ice cement, only seasonal frost; $n = 7$), active layer (permafrost cutbanks or samples overlying permafrost; $n = 11$), and permafrost (ground containing ice cement; $n = 5$), rarefied to 4,500 OTU reads.

We compared soil geochemistry to examine differences between permafrost, active-layer, and nonpermafrost sediments (Table 2). On average, organic matter in permafrost samples had a slightly lower $\delta^{13}C$ value of $-28.13 \pm 1.29‰$ (measurement mean with uncertainty reported as one standard deviation) compared to $-26.89 \pm 1.21‰$ for active-layer samples and $-26.96 \pm 0.49‰$ for nonpermafrost samples. TOC was more strongly correlated with grain size than permafrost presence, with nonpermafrost, active-layer, and permafrost samples having mean TOC values of $2.61 \pm 2.49\%$, $14.22 \pm 19.44\%$, and $9.42 \pm 9.80\%$, respectively. TN exhibited similar variation within classes; nonpermafrost samples had a mean TN value of $0.21 \pm 0.12\%$, while active-layer and permafrost samples had values of $0.46 \pm 0.40\%$ and $0.58 \pm 0.45\%$, respectively. However, permafrost samples displayed TOC/TN ratios slightly higher than those of nonpermafrost samples and with less variability than in the active layer. Mean TOC/TN ratios for permafrost samples were 11.8 ± 5.3, while TOC/TN ratios were 21.1 ± 19.8 for active-layer samples and 17.1 ± 6.1 for nonpermafrost samples. Therefore, permafrost, active-layer, and nonpermafrost samples show a similar N content, potentially indicating that N bioavailability is insensitive to permafrost thaw by either deepening of the active layer or bank erosion in the Koyukuk floodplain.

Effects of river migration. The differences in microbial communities between permafrost, active-layer, and nonpermafrost samples were greater than the variability within river deposits grouped into coeval scroll bar complexes. Samples from pits 1 to 6 were taken in a transect moving away from the river shoreline within a single scroll bar complex; these exhibited similar relative abundances of taxa at the family level (Fig. 3). Similarly, bank 1 and core 1 samples were also taken from the same scroll bar complex that is currently being eroded by the river; again, samples taken from similar depths (Bank1-Peat and Core1-22-28; Bank1-120 and Core1-111-115) displayed similar microbial community compositions at the family level. In contrast, permafrost, active-

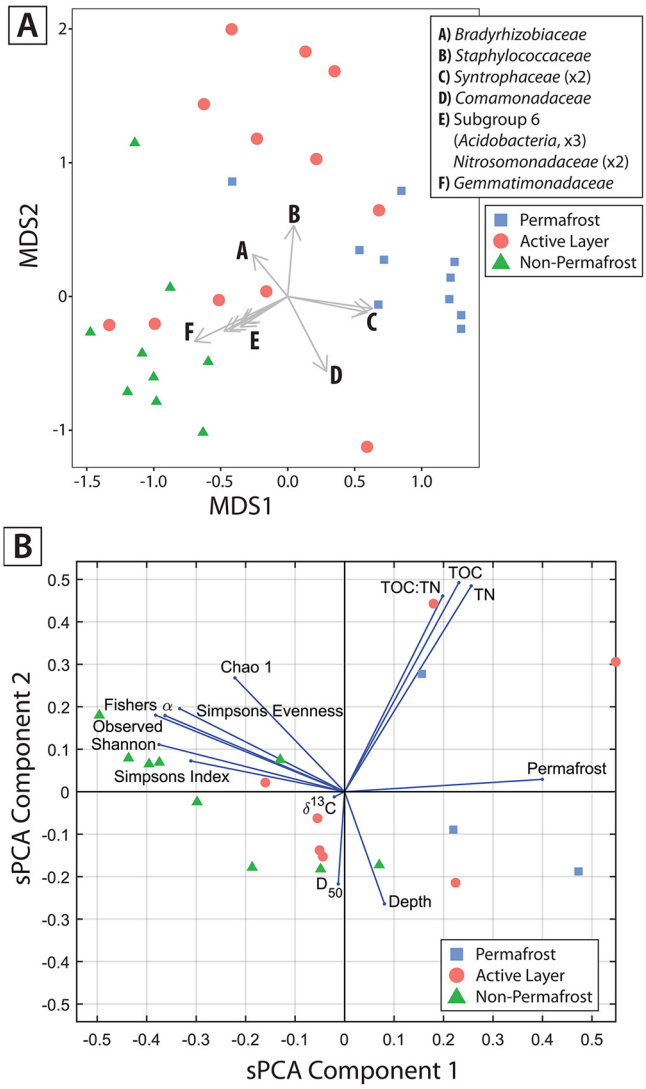

FIG 6 (A) NMDS analysis of microbial communities, color coded by sample classification as permafrost, active layer, or nonpermafrost, demonstrating that microbial communities vary depending on permafrost presence. The samples are plotted for MDS vectors from a Bray matrix calculated to maximize the difference between samples based on the rank order of the square root of taxon abundance for each sample. The vectors for OTUs with *P* values of $<10^{-5}$ are displayed, with the family-level taxonomic classification for each vector in the legend and the number of vectors for each family shown in parentheses. (B) Results of scaled principal-component analysis (sPCA), with diversity metrics for samples rarefied to 4,500 OTU reads, geochemical analyses, and metadata vectors plotted against the first and second principal components (accounting for 47% and 19% of sample variability, respectively).

layer, and nonpermafrost samples contained distinct communities, reflecting how variations in permafrost occurrence between scroll bar complexes govern microbial community, more so than variability within a scroll bar complex. Since scroll bar complex age and permafrost presence were strongly correlated, we were not able to deconvolve changes in microbial community due to deposit age from the presence or absence of permafrost.

To understand how river channel migration influences the geographic distribution of microbial communities, we compared samples from a permafrost section of floodplain and eroding riverbank to a nonpermafrost point bar (Fig. 7). As the Koyukuk River migrated, it eroded permafrost bank 9 while migrating toward core 9 (located on a distal permafrost floodplain approximately 5.5 km from the modern river channel) and depositing new sediment on the nonpermafrost opposing point bar at core 7 (Fig. 7).

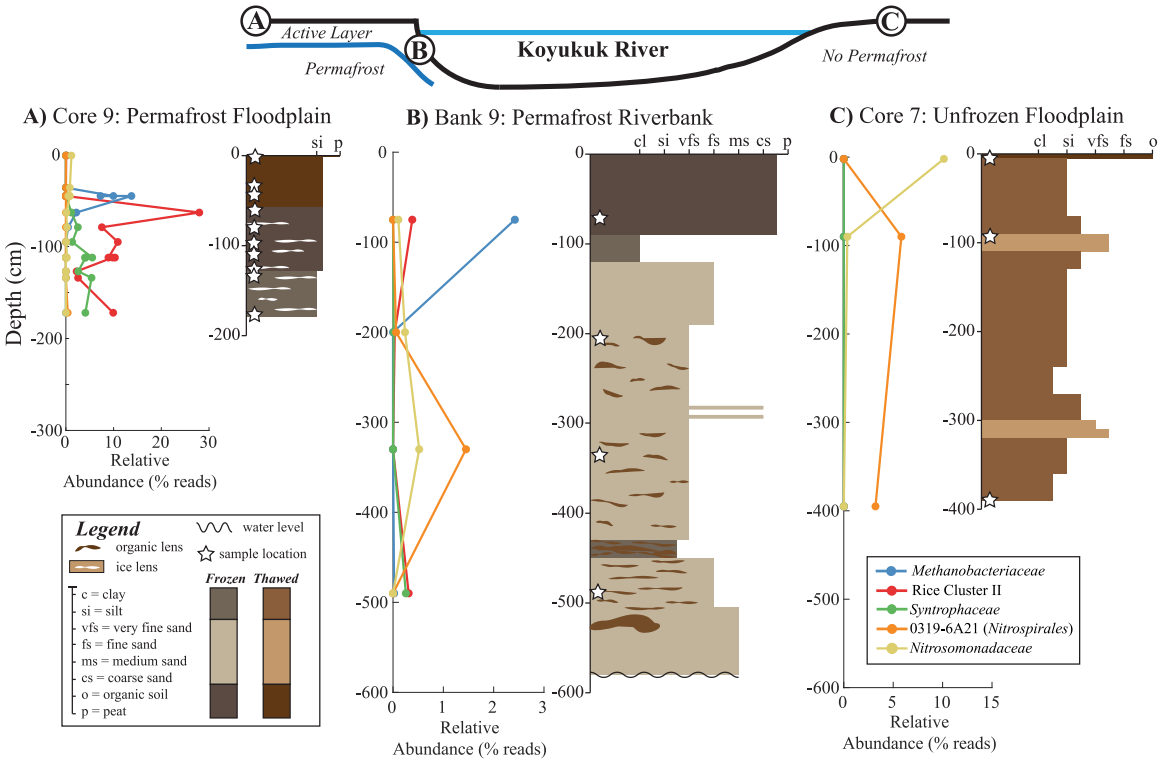

FIG 7 Idealized cross-section of the Koyukuk River. Steep, permafrost-bearing cutbanks were first thawed by the river, forming the active layer, before being eroded, and sediment is deposited on the opposing point bar without permafrost as the river migrates, maintaining approximately equal channel width. The locations of representative stratigraphic sections for our sampling locations across the permafrost floodplain (core 9; stratigraphic column A), permafrost riverbank (bank 9; stratigraphic column B), and nonpermafrost floodplain (core 7; stratigraphic column C) show sediment grain size classification versus depth. Grain size was classified in the field as clay (cl), silt (si), very fine sand (vf), fine sand (f), medium sand (m), coarse sand (c), and organic matter-rich horizons. For each location, the relative abundances of selected orders inferred to be involved in methanogenesis (Rice Cluster II and *Methanobacteriaceae*), sulfate reduction (*Syntrophaceae*), nitrite oxidation (*Nitrospirales*), and nitrogen fixation (*Bradyrhizobiaceae*) are plotted against sample depth, with sampling locations shown as stars on the stratigraphic columns.

We observed high relative abundances of OTUs classified as Rice Cluster II and *Methanobacteriaceae* methanogens in addition to anaerobic *Syntrophaceae* on the permafrost floodplain (core 9), as well as greater relative amplification of the *mcrA* gene. In contrast, samples taken on a partially frozen cutbank (bank 9) and unfrozen point bar (core 7) contained lower abundances of Rice Cluster II, *Methanobacteriaceae*, and *Syntrophaceae* and much lower relative amplification of *mcrA*.

The only taxa associated with methane cycling in bank 9 were located closer to the surface in the stratigraphic column; this pattern may be because peat is more insulating than sand and can preserve low temperatures in the upper soil column, even as underlying sand is thawed and eroded by the river. Alternatively, an anoxic layer could be generated close to the surface of the thawed permafrost cutbank as aerobic and facultative anaerobic taxa become established and multiply in the newly thawed active-layer community. In contrast, expected nitrogen cyclers, such as members of the *Nitrospirales* and *Nitrosomonadaceae*, were rare in permafrost floodplain deposits (core 9) but more abundant in the river cutbank and point bar (bank 9 and core 7). *Nitrospirales* had slightly higher relative abundances with depth, and we did not observe a clear trend in *Nitrosomonadaceae* with depth. The scarcity of families associated with nitrogen cycling coincided with lower TOC/TN ratios in active-layer and nonpermafrost deposits. Our observations also indicated that riverbanks along the Koyukuk experienced thaw during summer months, forming a lateral active layer with much greater grain sizes and lower organic content than typical surface soil horizons.

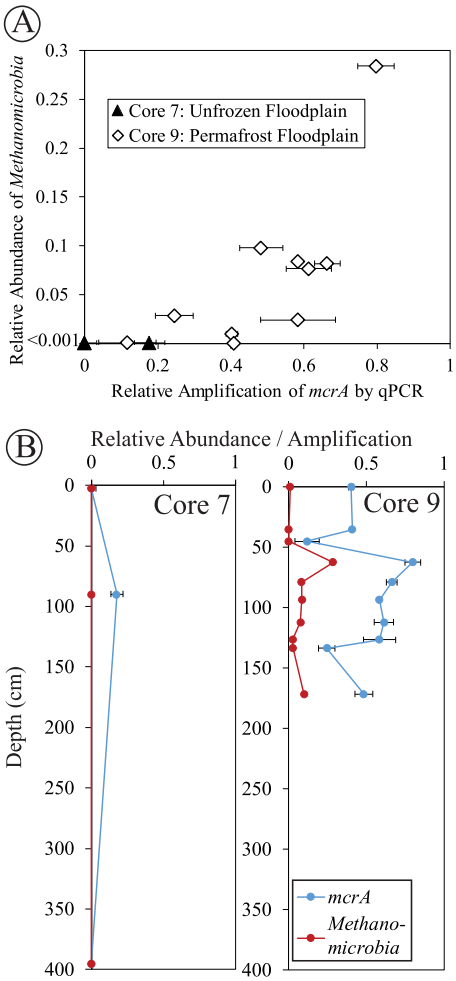

FIG 8 (A) Relative abundance of *Methanomicrobia* versus relative amplification of methyl-coenzyme M reductase (*mcrA*; functional gene for methanogenesis and anaerobic methanotrophy). Samples plotted at a relative abundance of <0.001 mark a bound indicating that no OTUs were assigned to *Methanomicrobia* taxa but that the samples may contain other taxa with the *mcrA* gene not assigned to *Methanomicrobia* or at very low abundance. Data for samples Core7-0-5 and Core7-390-400 overlap at the origin, and error bars represent 1 standard deviation. (B) Depth profiles of relative abundance of *Methanomicrobia* and relative amplification of *mcrA* from qPCR using the 16S rRNA gene as a control marker gene.

Therefore, the Koyukuk River introduces lateral heterogeneity in floodplain microbial communities by seasonally thawing its banks.

DISCUSSION

Mechanisms of community change. We found that samples taken from thawed river cutbanks have microbial communities similar to those in the active layer overlying permafrost deposits (Fig. 3). Since Arctic riverbanks erode at spatially variable rates up to meters per year (21)—in stark contrast to the deepening of the active layer overlying permafrost, which occurs at millimeters to centimeters per year (45)—cutbank thaw provides a natural experiment to evaluate the timescales of microbial community adjustment to permafrost thaw. Results indicated that microbial communities at the time of sampling (late June to early July 2018) had adjusted to unfrozen, well-drained, and aerobic conditions since the spring 2018 floods (May 2018). If microbial communities responded to permafrost thaw more slowly than the pace at which the river erodes its cutbank (which is approximately equal to the active-layer thickness per year), we would have seen samples taken on cutbanks with a microbial community structure similar to that in samples from the permafrost

TABLE 2 Chemical data for the sequenced sediment samples with $\pm 1\sigma$ uncertainty

Sample	TOC (wt%)	$\delta^{13}C$ (‰)	TN (wt%)	Molar TOC/TN ratio
Nonpermafrost				
Pit2-10	2.88 ± 0.07	−27.3 ± 0.1	0.22 ± 0.01	15.4 ± 0.8
Pit5-20	1.46 ± 0.04	−26.8 ± 0.1	0.18 ± 0.01	9.6 ± 0.5
Pit6-60	1.05 ± 0.03	−27.4 ± 0.1	0.12 ± 0.01	10.5 ± 0.6
Pit8-40	1.10 ± 0.03	−26.6 ± 0.1	0.14 ± 0.01	9.0 ± 0.5
Core7-0-5	7.74 ± 0.19	−27.7 ± 0.1	0.44 ± 0.02	20.6 ± 1.1
Core7-85-95	0.56 ± 0.01	−26.6 ± 0.1	0.10 ± 0.00	6.6 ± 0.4
Core7-390-400	5.25 ± 0.13	−26.2 ± 0.1	0.36 ± 0.02	17.0 ± 0.9
Bank2-10	3.20 ± 0.06	−27.3 ± 0.1	0.27 ± 0.02	13.9 ± 0.9
Bank2-230	0.27 ± 0.01	−26.7 ± 0.1	0.08 ± 0.01	3.8 ± 0.3
Active layer				
Bank1-Peat	6.45 ± 0.13	−27.1 ± 0.1	0.44 ± 0.03	17.2 ± 1.2
Core1-22-28	2.30 ± 0.05	−29.2 ± 0.1	0.26 ± 0.02	10.3 ± 0.7
Bank9-Peat	43.80 ± 0.86	−26.5 ± 0.1	1.03 ± 0.07	49.5 ± 3.3
Bank9-220	0.16 ± 0.00	−27.3 ± 0.1	0.05 ± 0.00	3.5 ± 0.2
Bank9-350	0.17 ± 0.00	−25.8 ± 0.1	0.05 ± 0.00	3.8 ± 0.3
Bank9-510	5.59 ± 0.11	−25.5 ± 0.1	0.44 ± 0.03	14.7 ± 1.0
Core9-33-38	41.07 ± 1.01	−26.8 ± 0.1	0.98 ± 0.05	48.9 ± 2.6
Permafrost				
Core1-105-111	3.50 ± 0.07	−29.6 ± 0.1	0.40 ± 0.03	10.3 ± 0.7
Core9-90-97	20.73 ± 0.51	−27.20 ± 0.1	1.09 ± 0.05	22.2 ± 1.2
Core9-169-174	4.04 ± 0.10	−27.6 ± 0.1	0.25 ± 0.01	18.7 ± 1.0

floodplain. Instead, calculated diversity indices (number of observed OTUs, Shannon diversity index, Chao 1, Simpson's index, and Fisher's alpha) showed that permafrost samples have lower diversity than active-layer and nonpermafrost samples (Fig. 5). The Simpson evenness values indicated that a few abundant taxa dominate permafrost environments but a characteristic active-layer community can develop within a single thaw season. Thus, we propose that samples from thawed, actively eroding permafrost cutbanks, showing more species and a higher Simpson evenness (such as samples from bank 1, bank 2, and bank 9), likely developed active-layer communities more rapidly than the river could erode newly thawed cutbank sediment. This interpretation agrees with incubation studies that found that microbial communities in thawing permafrost and active-layer samples converged on a timescale of days (46).

While motile or rapidly reproducing microbes may be able to change the makeup of a microbial community on small, incubation spatial scales, the transport of water and sediment across river floodplains may similarly help transport active-layer communities to newly thawed permafrost. For unfrozen channel banks directly in contact with the river, microbes transported by the river itself or pore fluid flow may homogenize bank microbial communities. Another mechanism that may help homogenize microbial communities not in contact with the river is cryoturbation, where seasonal freeze-thaw cycles physically mix floodplain sediments.

Importance of landscape heterogeneity. We found that OTU diversity decreases from the active layer to permafrost—a pattern consistent with previous studies (12, 39, 47). However, we discovered that thawed riverbank samples were more similar in OTU diversity to samples from the floodplain active layer than samples taken from permafrost at a similar depth below the ground surface (Fig. 7). Permafrost samples generally had a lower number of OTU reads than nonpermafrost samples from active layers, though our approach is not calibrated to provide a quantitative metric of absolute abundance. While some methanogens were observed in the upper peat layer of bank 9, deeper unfrozen sandy samples more closely resembled the nonpermafrost point bar sampled in core 7. Therefore, we argue that as the Koyukuk migrates and exposes deposits that had been previously buried meters underground to surface conditions,

this thawing disrupts permafrost microbial communities. These initial results suggest the interpretation that heterogeneous thaw and erosion of permafrost landscapes can disrupt established vertical trends in microbial diversity and community composition.

Effect of river channel migration on carbon cycling. We observed abundant methanogens in permafrost samples, including both hydrogenotrophic and acetoclastic taxa; this contrasted with only rare observations of methanogenic OTUs in nonpermafrost deposits. The occurrence of both acetoclastic and hydrogenotrophic methanogenic pathways has been globally documented in permafrost environments (48–50). We observed methanogen abundance from 16S classification peaking near the base of the active layer, in agreement with some previous studies (10, 15, 36, 51). However, the active layer of core 9 contained *mcrA* genes amplified by qPCR (Fig. 8), which may indicate the presence of methanogens throughout the sediment column, possibly due to interannual variability in the active-layer thickness or relict environmental DNA (eDNA) persisting in the deposits. We also found fewer methanotrophs in core 9, though they were relatively abundant in bank 1, which may indicate a lack of methanotrophs in the soil column (possibly due to a high water table) or that our vertical sampling intervals are too coarse to pick specific depths at which methanotrophs might have been more abundant (52). We emphasize that our study did not include direct measurements of the absolute abundance or activity of methane cycling within our samples. Further work is therefore required to determine if the stark differences observed in the relative abundance of methane cycling taxa between permafrost and nonpermafrost river sediment translate into absolute differences in the methane fluxes as river migration transforms this landscape (14).

Since only permafrost samples contained abundant methanogens and methanotrophs, and spatial patterns of Koyukuk River migration control the distribution of permafrost and nonpermafrost environments, we propose that river migration influences the fraction of floodplain area with potential for microbial methane cycling. River channel migration alters microbial communities in the Koyukuk River floodplain, giving insight into the floodplain's potential to respire CO_2 and methane in a warming climate. While we found evidence for methane cycling taxa only in older floodplain deposits that contained permafrost, all samples contained abundant anaerobic taxa. Therefore, we anticipate that river erosion of permafrost deposits will gradually decrease the area of the floodplain with potential to release methane. The taxa that we observed in point bar deposits would instead remineralize newly thawed carbon as CO_2, though likely at a low rate due to their anaerobic conditions and cold average temperatures, generating a weaker positive feedback to climate warming due to permafrost thaw (53, 54). For instance, if thawing permafrost destabilizes Arctic riverbanks (23), causing bank erosion rates to double, we expect that rivers would more rapidly decrease the floodplain area with significant relative abundance of methanogens, though at less than double the previous rate, as rivers tend to preferentially rework deposits near the channel (19). Our observations provide a framework and opportunity for future studies to use patterns of river channel migration to examine the influence of active landscape change on potential climate feedbacks in the Arctic.

Conclusions. In order to determine the effects of river channel migration on microbial communities in discontinuous permafrost floodplains, we collected samples from the Koyukuk River floodplain and investigated differences in microbial community compositions across the landscape using 16S amplicon sequencing and qPCR. Spatial patterns of river migration allowed us to evaluate how the floodplain microbial communities are responding to ongoing thaw and erosion of permafrost soils and deposition of unfrozen river sediment. We found that permafrost samples had lower microbial community diversity and evenness than active-layer and nonpermafrost samples, as well as higher TOC/TN ratios. During summer months, thawed channel banks develop an active-layer microbiome distinct from that of unthawed permafrost deposits found at a similar depth, suggesting that permafrost microbial communities adjust to thawed conditions in active-layer communities within the timescale of river cutbank thaw and erosion. Among these distinctions, we noted that methanogens and methanotrophs are abundant in permafrost samples and rare in active-layer and

nonpermafrost sediments and that this interpretation was supported by the relationship between relative amplification of the *mcrA* functional gene and abundance of taxa assigned to the *Methanomicrobia*. Therefore, the cadence and spatial pattern of river migration influence the rate of change of microbial communities with potential roles in biogeochemical cycling, for instance, by eroding the floodplain area that hosts microbial communities with potential for substantial methane cycling.

MATERIALS AND METHODS

Field site. The Koyukuk River is a major tributary of the Yukon River and runs south from its headwaters in the Brooks Range, meandering through discontinuous permafrost in the west-central Alaska lowlands (26) (Fig. 1A). The region had an arid climate during the last ice age and was unglaciated, instead hosting a more extensive predecessor of the modern Nogahabara dune field (27). In the present day, permafrost typically underlies black spruce, birch-ericaceous shrubs, and tussock sedge bogs in wet soils with thick upper strata of peat that can extend more than 1 m below the surface. Nonpermafrost areas contain denser stands of white spruce, balsam poplar, alder, and willow trees in well-drained locations and form wet sedge meadows in saturated soils (26). The vegetation on the Koyukuk floodplain highlights the topography of successive abandoned levees known as scroll bars (28), with trees growing on the ridges and grasses and moss occupying the troughs between successive levees (Fig. 1C). The floodplain contains numerous lakes, and soils are frequently saturated. The region experiences wildfires with an approximately 180-year recurrence interval, and microbial communities in the underlying deposits have been potentially impacted by fires through combustion of upper-soil organic horizons and a temporary increase in active-layer thickness (29).

Our field sampling centered on the Koyukuk River floodplain near the village of Huslia (Fig. 1A). Huslia has a mean annual temperature of −3.6°C and mean annual precipitation of 31 cm/year rainfall or snow water equivalent, measured from 1981 to 2010 (30, 31). Analysis of Landsat imagery indicated that the Koyukuk channel migrates at rates up to 11 m/year, with average rates of 0.53 m/year in the reach indicated in Fig. 1B (21). The highest erosion rates occurred at the apices of the more tightly curved meander bends.

Field sampling. We collected samples on the Koyukuk River floodplain near Huslia, AK, in June and July of 2018 (Fig. 1A). During sampling, we measured a mean thaw depth of approximately 0.75 m, with a range from 0.40 m to over 1.00 m, based on cores and surveys with a 1-m-long permafrost probe. We classified samples taken from cores as permafrost versus seasonal frost by the presence of ice cement and frozen material without thawed intervals at depths greater than 1 m, in contrast to observed intervals of seasonal frost ~0.2 m thick at a <2-m depth that did not contain ice cement and had thawed sediment both above and below them.

Samples of channel banks and shallow unfrozen sediment were collected using a hand trowel (bank 1, bank 2, and bank 9 samples, collected from cutbanks; pit 1, pit 2, pit 5, pit 6, and pit 8 samples, collected on active point bars), deep unfrozen cores were collected using a hand auger (core 7), and frozen cores were collected using a gas-powered US Snow, Ice and Permafrost Research Establishment (SIPRE) corer and split in the field on a plastic tarp using a hacksaw (core 1 and core 9 samples). Sample sites were chosen to include floodplain areas with different relative ages, which were defined based on cross-cutting relationships between scroll bar sets in aerial images (Fig. 1B and C). Scroll bars are levees abandoned through channel lateral migration that tend to record the approximate location of the river inner bank through time, though a single scroll develops over multiple flood events and does not record a single instance of formation (Fig. 1E) (25). In contrast, to compare microbial communities within a single scroll bar complex, pits 1, 2, 5, and 6 were sampled along a transect perpendicular to the river centerline, extending from the point bar. Sampling locations were chosen to include permafrost and unfrozen deposits, as well as material from the riverbank and floodplain spanning the youngest (PB1 and PB2) to oldest (core 9) mappable units on the floodplain within constraints required for access by boat. Sample collection extended up to a 4-m depth, and sampling depths were selected after characterizing the stratigraphic section to span the grain size and sedimentological units present at each location (Table 3). Nitrile gloves were worn during sample collection, and sampling implements were rinsed with deionized water between samples. Samples were refrigerated in coolers in the field and transferred to an ice chest in the evening, before being flown back to the laboratory in coolers and stored in a cold room at −15°C. The core 1 samples showed signs of partial thaw during transport from the field; we estimate that the samples were potentially unfrozen for up to about 8 h.

Deposit characteristics. Each sample was dried in precombusted Al foil at 55 to 60°C, then gently homogenized in a mortar and pestle, and subsampled using a riffle splitter. Prior to grain size analysis, samples were treated to remove carbonate and organic material (55). A sample split was decarbonated in 1 M HCl in a sterile polypropylene Falcon tube, centrifuged for 15 min at 4,000 rpm, and then decanted by hand. Each sample was then rinsed twice with ~45 ml of deionized (DI) H_2O, centrifuged, and decanted before redrying of the Falcon tubes in the oven at 55 to 60°C. To remove organic matter, each sample was transferred to a Pyrex beaker sitting at 85°C on a hot plate and treated with 20 ml of 30% H_2O_2 until oxidation reactions ceased (based on visual inspection of bubbling). Larger, floating organic matter was removed using a microspatula. After removal of organic matter, each sample was transferred back into its original Falcon tube and rinsed three times with centrifuging and decanting before being dried in the oven. Sediment grain size distribution was measured using laser diffraction. DI water and Calgon were added to each sample to rehydrate and prevent flocking; clumps of sediment were broken

TABLE 3 Sample location metadata, with median grain size measured using laser diffraction

Sample	Permafrost classification	Depth (cm)	Median grain size (μm)	Sediment class	Landform
Pit1-1	Nonpermafrost	1		Silt[a]	Point Bar
Pit2-10	Nonpermafrost	10	70.664	Sand	Point Bar
Pit5-20	Nonpermafrost	20	24.262	Silt	Point Bar
Pit6-0	Nonpermafrost	Surface		Silt[a]	Point Bar
Pit6-60	Nonpermafrost	60	90.390	Sand	Point Bar
Pit8-40	Nonpermafrost	40	32.250	Silt	Point Bar
Core7-0-5	Nonpermafrost	2	17.669	Topsoil	Floodplain
Core7-85-95	Nonpermafrost	90	56.611	Silt	Floodplain
Core7-390-400	Nonpermafrost	395	57.561	Silt	Floodplain
Bank2-10	Nonpermafrost	10	33.413	Silt	Bank
Bank2-230	Nonpermafrost	230	111.183	Sand	Bank
Bank1-Peat	Active layer	35	9.139	Peat	Bank
Bank1-120	Active layer	120	10.685	Silt	Bank
Core1-22-28	Active layer	25	10.101	Silt	Floodplain
Core1-105-111	Permafrost	108	10.718	Silt	Floodplain
Bank9-Peat	Active layer	75	47.659	Peat	Bank
Bank9-220	Active layer	200	207.325	Sand	Bank
Bank9-350	Active layer	330	154.874	Sand	Bank
Bank9-510	Active layer	490	52.863	Silt	Bank
Core9-0	Active layer	Surface		Peat[a]	Floodplain
Core9-33-38	Active layer	35	51.129	Peat	Floodplain
Core9-44-46-R1	Active layer	45		Peat[a]	Floodplain
Core9-44-46-R2	Active layer	45		Peat[a]	Floodplain
Core9-44-46-R3	Active layer	45		Peat[a]	Floodplain
Core9-58-67	Permafrost	63		Peat[a]	Floodplain
Core9-75-83	Permafrost	79		Peat[a]	Floodplain
Core9-90-97	Permafrost	95	16.947	Peat	Floodplain
Core9-109-115-R1	Permafrost	112		Peat[a]	Floodplain
Core9-109-115-R2	Permafrost	112		Peat[a]	Floodplain
Core9-109-115-R3	Permafrost	112		Peat[a]	Floodplain
Core9-123-130	Permafrost	127		Peat[a]	Floodplain
Core9-130-137	Permafrost	134		Silt[a]	Floodplain
Core9-169-174	Permafrost	172	28.044	Silt	Floodplain

[a]Sediment class based on field observations; grain size not measured using laser diffraction.

up by sonicating each sample for 3 min. The samples were then split while wet and run for grain size on a Malvern Mastersizer 2000, calibrated using a laboratory silica carbide standard. Replicate analysis of the silica carbide standard yielded a median grain diameter (D_{50}), of 13.184 $\pm$ 0.105 μm.

Total organic carbon (TOC), stable carbon isotope ratios, and total nitrogen (TN) were measured from dried sample splits. Approximately 3 mg of each sample was weighed out into a silver capsule. The sample was acidified by fumigation with HCl, and then carbon and nitrogen content and carbon stable isotopes were measured on a Costech elemental analyzer coupled to a MAT 253 isotope ratio mass spectrometer (IRMS). Isotope ratios ($R = {}^{13}C/{}^{12}C$) are reported in standard notation relative to Vienna Pee Dee Belemnite (VPDB) [$\delta^{13}C = (R_{sample}/R_{VPDB}) - 1$, reported in per mille]. The measurements were calibrated using laboratory standards of peach leaves (1570a; TOC = 44.65%, measured at 44.33 $\pm$ 0.96%; $\delta^{13}C$ = $-$25.95‰, measured at $-$26.13 $\pm$ 0.08‰; TN = 2.83%, measured at 3.31 $\pm$ 1.27%), urea (Eurovector; TOC = 20.00% measured at 17.98 $\pm$ 0.37%; TN = 46.65% measured at 45.88 $\pm$ 0.88%) and 2,5-bis(5-tert-butyl-2-benzo-oxazol-2-yl) thiophene (BBOT; Eurovector; TOC = 72.53%, measured at 69.59 $\pm$ 2.05%; $\delta^{13}C$ = $-$26.6‰, measured at $-$26.6 $\pm$ 0.01‰; TN = 6.51%, measured at 6.82 $\pm$ 0.24%) for TOC and TN and cellulose (IAEA-C3; $\delta^{13}C$ = $-$24.91‰, measured at $-$24.82 $\pm$ 0.06‰), sucrose (IAEA-C6; $\delta^{13}C$ = $-$10.8‰, measured at $-$10.7 $\pm$ 0.03‰), and oxalic acid (IAEA-C8; $\delta^{13}C$ = $-$18.3‰, measured at $-$18.5 $\pm$ 0.06‰) for C stable isotopes. Measured blanks were below peak detection limit.

DNA extraction. To characterize variations in microbial community across the Koyukuk floodplain, small subsamples were collected for DNA extraction after bulk samples were thawed overnight at 4°C and before core homogenization for geochemistry measurements. To assess microbial community variability within a single core, evaluate sequencing reproducibility, and assess the potential for contamination during field sampling, multiple subsamples were collected from the same 1-cm interval within core 9. For each sample, ~250 mg of sediment was bead beaten in a DNA stabilization buffer (DNA/RNA Shield in BashingBead lysis tubes; Zymo) to dislodge and lyse microbial cells associated with the sediment. Samples were frozen for up to 6 weeks between bead beating and DNA extraction. Upon thawing, DNA was extracted from the lysate using a soil/fecal DNA miniprep kit (Zymo). Procedural blanks were run alongside the samples to characterize contamination during DNA extraction and amplification.

Amplification and sequencing. A segment of the V4-to-V5 hypervariable region of the 16S rRNA gene was amplified by PCR using archaeal/bacterial primers 515f and 926r (56), with Illumina adapters

on the 5′ ends. PCRs were set up in 15-μl volumes with Q5 Hot Start high-fidelity 2× master mix (New England Biolabs), with annealing at 54°C and 30 cycles. Selected samples (Core9-44-46-R1, Core9-44-46-R3, Core9-58-67, Core9-75-83, Core9-109-115-R1, Core9-109-115-R2, and Core9-109-115-R3) were diluted 10× with MilliQ water before amplification after an initial amplification generated faint bands during PCR amplification.

A 2.5-μl portion of each product was barcoded with Illumina Nextera XT index 2 primers that include unique 8-bp barcodes (P5 5′-AATGATACGGCGACCACCGAGATCTACACXXXXXXXXTCGTCGGCAGCGTC-3′ and P7 5′-CAAGCAGAAGACGGCATACGAGATXXXXXXXXGTCTCGTGGGCTCGG-3′). PCR amplification with barcoded primers was conducted in 25-μl reactions with annealing at 66°C and 10 cycles.

Barcoded products were purified using a Millipore-Sigma MultiScreen plate with vacuum manifold and quantified using the Thermo Fisher Scientific QuantIT PicoGreen double-stranded DNA (dsDNA) assay kit on the Bio-Rad CFX96 Touch real-time PCR detection system. Barcoded samples were combined in equimolar amounts in a single tube and purified with a Qiagen PCR purification kit before submission to Laragen for 2 × 250-bp paired-end analysis on Illumina's MiSeq platform.

qPCR. Quantitative real-time PCR (qPCR) was conducted on samples from core 9 and core 7 to examine the presence and abundance of methyl-coenzyme M reductase (MCR), encoded by a functional marker gene commonly used to assess methane cycling in environmental samples (57, 58). Quantitative PCRs were conducted in 10 μl volumes with iTaq universal SYBR green supermix (Bio-Rad), using the MCR a-subunit (*mcrA*) primers ME1 and ME2 (59), with parallel reactions using the 16S primers described above. Reactions were run in triplicate in a CFX96 real-time PCR detection system (Bio-Rad), with an initial denaturation step of 3 min followed by 39 cycles of 10 s denaturation at 95°C and 30 s annealing/extension at 55°C. Fluorescence readout was measured following each cycle, and the cycle at which the target gene crossed the threshold of a detectable amplification curve (C_q) was determined using the CFX Manager software (Bio-Rad). C_q values were normalized to negative controls for each target gene ($\Delta C_q = C_{q\_neg} - C_{q\_sample}$), and *mcrA* was normalized to 16S ($\Delta C_{q\_MCR}/\Delta C_{q\_16S}$).

Data processing. Sequence data were processed using QIIME version 1.8.0 (60) following a previously published protocol (61). Raw sequence pairs were joined and quality trimmed using the default parameters in QIIME. Sequences were clustered into *de novo* operational taxonomic units (OTUs) with 97% similarity using the UCLUST open reference clustering protocol. Clustering sequences using the same protocol at 99% similarity did not significantly change OTU assignments or the main results of our analysis. The most abundant sequence was chosen as representative for each *de novo* OTU (62). Taxonomic identification for each representative sequence was assigned using the Silva-119 database (63). Tables of both absolute and relative abundance were generated for each sample. To further interrogate taxonomy of certain OTUs, we compared their representative sequences against the National Institutes of Health (NIH) BLASTn database using a standard nucleotide BLAST for highly similar sequences using the Megablast algorithm on 24 September 2019.

Before analysis of microbial community trends across environment and depth, the *de novo* OTUs were singleton filtered, and unassigned and eukaryotic OTUs were removed. In addition, OTUs with over 50 reads in each respective extraction and amplification blank were removed. Nonmetric multidimensional scaling (NMDS) plots were constructed using the vegan ecology package in RStudio for a Bray dissimilarity matrix calculated based on the square root of taxon abundance. NMDS plots were generated by rank ordering *n* OTUs present in different samples and projecting the samples on the plane in *n*-dimensional space defined by the two vectors accounting for most of the variation in the sample set. The OTU vectors on each NMDS plot were extracted using the envfit function from vegan, run for 99,999 permutations. We plotted the NMDS with vectors of *de novo* OTUs with *P* values less than 10^{-5}.

Alpha diversity calculations (observed OTUs, Shannon diversity index, Chao 1, Fisher's alpha, Simpson's index, and Simpson's evenness) were carried out in QIIME1.8.0 (alpha_diversity.py), on data sets rarefied by random subsampling to a consistent depth (single_rarefaction.py). Figures and results presented used data sets rarefied to 4,500 counts (5 permafrost, 11 active-layer, and 7 nonpermafrost samples), but a similar pattern was obtained by rarefying to 1,000 counts (10 permafrost, 14 active-layer, and 9 nonpermafrost samples). The diversity metrics calculated using data sets rarefied to 4,500 counts were compared to soil chemistry and sampling location metadata using scaled principal-component analysis (sPCA) in Matlab 2018b.

This sequencing approach does not distinguish active cells from dead or extracellular DNA and in some examples has been shown to underestimate the abundance of certain taxa and functional groups, particularly *Deltaproteobacteria* and *Firmicutes* (64, 65). Fully characterizing microbial activity and absolute abundance under present and changing climatic conditions requires qPCR and live/dead assays from incubations in addition to *in situ* measurements of redox conditions and gas fluxes (15, 48, 66). However, recent work quantifying the abundance of live, dead, and dormant cells across a permafrost chronosequence indicated that removal of DNA from dead cells did not significantly change taxonomic relative abundance down to the family level, despite a significant decrease in 16S rRNA gene reads after treatment with increasing permafrost age (48). Our field sampling also captured a snapshot of the landscape before peak thaw in late summer and thus did not address potential seasonal changes in the microbial communities. Based on previous work on monthly variation seen by 16S sequencing of permafrost on Svalbard, we may have overestimated the abundance of *Cyanobacteria*, candidate division AD3 organisms, and *Alphaproteobacteria*, but other taxa are expected to exhibit little seasonal variation (67).

Data availability. All sequences are available at NCBI Sequence Read Archive, under BioProject accession number PRJNA728135.

SUPPLEMENTAL MATERIAL

Supplemental material is available online only.

SUPPLEMENTAL FILE 1, XLSX file, 8.8 MB.

ACKNOWLEDGMENTS

We thank the Koyukuk-hotana Athabascans, First Chief Norman Burgett, and the Huslia Tribal Council for access to their land and USFWS–Koyukuk National Wildlife refuge for research permitting and logistical assistance. Shawn Huffman, Alvin Attla, and Virgil Umphenour provided invaluable field logistical support and local expertise. Stephanie Connon helped with iTAG and sequencing preparation.

We acknowledge support from Foster and Coco Stanback, the Linde Family, the Caltech Terrestrial Hazards Observation and Reporting (THOR) Center, and the Caltech Center for Environmental Microbial Interactions (CEMI) for funding this research. M.M.D. and P.C.K. acknowledge support from the National Defense Science and Engineering Graduate Fellowship (NDSEG). P.C.K. acknowledges the Fannie and John Hertz Foundation Cohen/Jacobs and Stein Family Fellowship. U.F.L. acknowledges support of the National Science Foundation (GRFP). Support was also provided by the Department of Energy Office of Science, Biological and Environmental Research Subsurface Biogeochemical Research (SBR) Program Early Career award to J.C.R.

REFERENCES

1. Zhang T, Barry RG, Knowles K, Heginbottom JA, Brown J. 1999. Statistics and characteristics of permafrost and ground-ice distribution in the Northern Hemisphere. Polar Geogr 23:132–154. https://doi.org/10.1080/10889379909377670.
2. Schuur EG, McGuire AD, Schädel C, Grosse G, Harden JW, Hayes DJ, Hugelius G, Koven CD, Kuhry P, Lawrence DM, Natali SM, Olefeldt D, Romanovsky VE, Schaefer K, Turetsky MR, Treat CC, Vonk JE. 2015. Climate change and the permafrost carbon feedback. Nature 520:171–179. https://doi.org/10.1038/nature14338.
3. Jansson JK, Taş N. 2014. The microbial ecology of permafrost. Nat Rev Microbiol 12:414–425. https://doi.org/10.1038/nrmicro3262.
4. Serreze MC, Barry RG. 2011. Processes and impacts of Arctic amplification: a research synthesis. Glob Planet Chang 77:85–96. https://doi.org/10.1016/j.gloplacha.2011.03.004.
5. Schädel C, Bader MK-F, Schuur EAG, Biasi C, Bracho R, Čapek P, De Baets S, Diáková K, Ernakovich J, Estop-Aragones C, Graham DE, Hartley IP, Iversen CM, Kane E, Knoblauch C, Lupascu M, Martikainen PJ, Natali SM, Norby RJ, O'Donnell JA, Chowdhury TR, Šantrůčková H, Shaver G, Sloan VL, Treat CC, Turetsky MR, Waldrop MP, Wickland KP. 2016. Potential carbon emissions dominated by carbon dioxide from thawed permafrost soils. Nat Clim Chang 6:950–953. https://doi.org/10.1038/nclimate3054.
6. Monteux S, Weedon JT, Blume-Werry G, Gavazov K, Jassey VEJ, Johansson M, Keuper F, Olid C, Dorrepaal E. 2018. Long-term in situ permafrost thaw effects on bacterial communities and potential aerobic respiration. ISME J 12:2129–2141. https://doi.org/10.1038/s41396-018-0176-z.
7. Knoblauch C, Beer C, Sosnin A, Wagner D, Pfeiffer E-M. 2013. Predicting long-term carbon mineralization and trace gas production from thawing permafrost of Northeast Siberia. Glob Chang Biol 19:1160–1172. https://doi.org/10.1111/gcb.12116.
8. Knoblauch C, Beer C, Liebner S, Grigoriev MN, Pfeiffer E-M. 2018. Methane production as key to the greenhouse gas budget of thawing permafrost. Nat Clim Chang 8:309–312. https://doi.org/10.1038/s41558-018-0095-z.
9. Zona D, Gioli B, Commane R, Lindaas J, Wofsy SC, Miller CE, Dinardo SJ, Dengel S, Sweeney C, Karion A, Chang RY-W, Henderson JM, Murphy PC, Goodrich JP, Moreaux V, Liljedahl A, Watts JD, Kimball JS, Lipson DA, Oechel WC. 2016. Cold season emissions dominate the Arctic tundra methane budget. Proc Natl Acad Sci U S A 113:40–45. https://doi.org/10.1073/pnas.1516017113.
10. Barbier BA, Dziduch I, Liebner S, Ganzert L, Lantuit H, Pollard W, Wagner D. 2012. Methane-cycling communities in a permafrost-affected soil on Herschel Island, Western Canadian Arctic: active layer profiling of mcrA and pmoA genes. FEMS Microbiol Ecol 82:287–302. https://doi.org/10.1111/j.1574-6941.2012.01332.x.
11. Treat CC, Marushchak ME, Voigt C, Zhang Y, Tan Z, Zhuang Q, Virtanen TA, Räsänen A, Biasi C, Hugelius G, Kaverin D, Miller PA, Stendel M, Romanovsky V, Rivkin F, Martikainen PJ, Shurpali NJ. 2018. Tundra landscape heterogeneity, not interannual variability, controls the decadal regional carbon balance in the Western Russian Arctic. Glob Chang Biol 24:5188–5204. https://doi.org/10.1111/gcb.14421.
12. Taş N, Prestat E, Wang S, Wu Y, Ulrich C, Kneafsey T, Tringe SG, Torn MS, Hubbard SS, Jansson JK. 2018. Landscape topography structures the soil microbiome in arctic polygonal tundra. Nat Commun 9:777. https://doi.org/10.1038/s41467-018-03089-z.
13. Kuhn M, Lundin EJ, Giesler R, Johansson M, Karlsson J. 2018. Emissions from thaw ponds largely offset the carbon sink of northern permafrost wetlands. Sci Rep 8:9535–9537. https://doi.org/10.1038/s41598-018-27770-x.
14. McCalley CK, Woodcroft BJ, Hodgkins SB, Wehr RA, Kim E-H, Mondav R, Crill PM, Chanton JP, Rich VI, Tyson GW, Saleska SR. 2014. Methane dynamics regulated by microbial community response to permafrost thaw. Nature 514:478–481. https://doi.org/10.1038/nature13798.
15. Liebner S, Ganzert L, Kiss A, Yang S, Wagner D, Svenning MM. 2015. Shifts in methanogenic community composition and methane fluxes along the degradation of discontinuous permafrost. Front Microbiol 6:356. https://doi.org/10.3389/fmicb.2015.00356.
16. Mondav R, Woodcroft BJ, Kim E-H, McCalley CK, Hodgkins SB, Crill PM, Chanton J, Hurst GB, VerBerkmoes NC, Saleska SR, Hugenholtz P, Rich VI, Tyson GW. 2014. Discovery of a novel methanogen prevalent in thawing permafrost. Nat Commun 5:3212. https://doi.org/10.1038/ncomms4212.
17. Lininger KB, Wohl E. 2019. Floodplain dynamics in North American permafrost regions under a warming climate and implications for organic carbon stocks: a review and synthesis. Earth-Science Rev 193:24–44. https://doi.org/10.1016/j.earscirev.2019.02.024.
18. Torres MA, Kemeny PC, Lamb MP, Cole TL, Fischer WW. 2020. Long-term storage and age-biased export of fluvial organic carbon: field evidence from West Iceland. Geochem Geophys Geosyst 21:e2019GC008632. https://doi.org/10.1029/2019GC008632.
19. Torres MA, Limaye AB, Ganti V, Lamb MP, West AJ, Fischer WW. 2017. Model predictions of long-lived storage of organic carbon in river deposits. Earth Surf Dynam 5:711–730. https://doi.org/10.5194/esurf-5-711-2017.
20. Shur YL, Jorgenson MT. 2007. Patterns of permafrost formation and degradation in relation to climate and ecosystems. Permafrost Periglac Process 18:7–19. https://doi.org/10.1002/ppp.582.
21. Rowland J, Stauffer S, Schwenk J. 2019. Pan-arctic river bank erosion and accretion, and planform metrics measured over intervals ranging from 1973 to 2016. Incorporating the hydrological controls on carbon cycling in floodplain ecosystems into earth system models (ESMs). https://data.ess-dive.lbl.gov/view/doi:10.15485/1571527.

22. Mann DH, Fastie CL, Rowland EL, Bigelow NH. 1995. Spruce succession, disturbance, and geomorphology on the Tanana River floodplain, Alaska. Ecoscience 2:184–199. https://doi.org/10.1080/11956860.1995.11682283.
23. Costard F, Dupeyrat L, Gautier E, Carey-Gailhardis E. 2003. Fluvial thermal erosion investigations along a rapidly eroding river bank: application to the Lena River (central Siberia). Earth Surf Process Landforms 28:1349–1359. https://doi.org/10.1002/esp.592.
24. Costard F, Gautier E, Fedorov A, Konstantinov P, Dupeyrat L. 2014. An assessment of the erosion potential of the fluvial thermal process during ice breakups of the Lena River (Siberia). Permafrost Periglac Process 25:162–171. https://doi.org/10.1002/ppp.1812.
25. Miall AD. 1990. Principles of sedimentary basin analysis, 2nd ed. Springer, New York, NY.
26. Nowacki GJ, Spencer P, Fleming M, Brock T, Jorgenson T. 2003. Unified ecoregions of Alaska: 2001. 2002–297. USGS Numbered Series. U.S. Geological Survey, Reston, VA.
27. Barclay DJ, Wiles GC, Calkin PE. 2009. Holocene glacier fluctuations in Alaska. Quat Sci Rev 28:2034–2048. https://doi.org/10.1016/j.quascirev.2009.01.016.
28. Mason J, Mohrig D. 2019. Scroll bars are inner bank levees along meandering river bends. Earth Surf Process Landforms 44:2649–2659. https://doi.org/10.1002/esp.4690.
29. O'Donnell JA, Jorgenson MT, Harden JW, McGuire AD, Kanevskiy MZ, Wickland KP. 2012. The effects of permafrost thaw on soil hydrologic, thermal, and carbon dynamics in an Alaskan peatland. Ecosystems 15:213–229. https://doi.org/10.1007/s10021-011-9504-0.
30. Daly C, Smith JI, Olson KV. 2015. Mapping atmospheric moisture climatologies across the conterminous United States. PLoS One 10:e0141140. https://doi.org/10.1371/journal.pone.0141140.
31. Daly C, Smith J, Halbleib M. 2018. Data from "1981–2010 High-Resolution Temperature and Precipitation Maps for Alaska Final Report." PRISM Climate Group, Oregon State University, Corvallis, OR. http://www.prism.oregonstate.edu/projects/public/alaska/grids/.
32. Kim HM, Lee MJ, Jung JY, Hwang CY, Kim M, Ro H-M, Chun J, Lee YK. 2016. Vertical distribution of bacterial community is associated with the degree of soil organic matter decomposition in the active layer of moist acidic tundra. J Microbiol 54:713–723. https://doi.org/10.1007/s12275-016-6294-2.
33. Galushko A, Kuever J. 2019. Syntrophus, p 1–6. *In* Bergey's manual of systematics of Archaea and Bacteria. Wiley Online Library.
34. Yamada T, Sekiguchi Y. 2018. Anaerolineaceae, p 1–5. *In* Bergey's manual of systematics of Archaea and Bacteria. Wiley Online Library.
35. Allan J, Ronholm J, Mykytczuk NCS, Greer CW, Onstott TC, Whyte LG. 2014. Methanogen community composition and rates of methane consumption in Canadian High Arctic permafrost soils. Environ Microbiol Rep 6:136–144. https://doi.org/10.1111/1758-2229.12139.
36. Kotsyurbenko OR, Chin K-J, Glagolev MV, Stubner S, Simankova MV, Nozhevnikova AN, Conrad R. 2004. Acetoclastic and hydrogenotrophic methane production and methanogenic populations in an acidic West-Siberian peat bog. Environ Microbiol 6:1159–1173. https://doi.org/10.1111/j.1462-2920.2004.00634.x.
37. Haroon MF, Hu S, Shi Y, Imelfort M, Keller J, Hugenholtz P, Yuan Z, Tyson GW. 2013. Anaerobic oxidation of methane coupled to nitrate reduction in a novel archaeal lineage. Nature 500:567–570. https://doi.org/10.1038/nature12375.
38. Johnston ER, Hatt JK, He Z, Wu L, Guo X, Luo Y, Schuur EAG, Tiedje JM, Zhou J, Konstantinidis KT. 2019. Responses of tundra soil microbial communities to half a decade of experimental warming at two critical depths. Proc Natl Acad Sci U S A 116:15096–15105. https://doi.org/10.1073/pnas.1901307116.
39. Lipson DA, Raab TK, Parker M, Kelley ST, Brislawn CJ, Jansson J. 2015. Changes in microbial communities along redox gradients in polygonized Arctic wet tundra soils. Environ Microbiol Rep 7:649–657. https://doi.org/10.1111/1758-2229.12301.
40. Steinberg LM, Regan JM. 2009. mcrA-targeted real-time quantitative PCR method to examine methanogen communities. Appl Environ Microbiol 75:4435–4442. https://doi.org/10.1128/AEM.02858-08.
41. Blake LI, Tveit A, Øvreås L, Head IM, Gray ND. 2015. Response of methanogens in Arctic sediments to temperature and methanogenic substrate availability. PLoS One 10:e0129733. https://doi.org/10.1371/journal.pone.0129733.
42. Hilton RG, Galy V, Gaillardet J, Dellinger M, Bryant C, O'Regan M, Gröcke DR, Coxall H, Bouchez J, Calmels D. 2015. Erosion of organic carbon in the Arctic as a geological carbon dioxide sink. Nature 524:84–87. https://doi.org/10.1038/nature14653.
43. Galy V, France-Lanord C, Lartiges B. 2008. Loading and fate of particulate organic carbon from the Himalaya to the Ganga–Brahmaputra delta. Geochim Cosmochim Acta 72:1767–1787. https://doi.org/10.1016/j.gca.2008.01.027.
44. Zhang X, Xu S, Li C, Zhao L, Feng H, Yue G, Ren Z, Cheng G. 2014. The soil carbon/nitrogen ratio and moisture affect microbial community structures in alkaline permafrost-affected soils with different vegetation types on the Tibetan plateau. Res Microbiol 165:128–139. https://doi.org/10.1016/j.resmic.2014.01.002.
45. Luo D, Wu Q, Jin H, Marchenko SS, Lü L, Gao S. 2016. Recent changes in the active layer thickness across the northern hemisphere. Environ Earth Sci 75:555. https://doi.org/10.1007/s12665-015-5229-2.
46. Mackelprang R, Waldrop MP, DeAngelis KM, David MM, Chavarria KL, Blazewicz SJ, Rubin EM, Jansson JK. 2011. Metagenomic analysis of a permafrost microbial community reveals a rapid response to thaw. Nature 480:368–371. https://doi.org/10.1038/nature10576.
47. Yergeau E, Hogues H, Whyte LG, Greer CW. 2010. The functional potential of high Arctic permafrost revealed by metagenomic sequencing, qPCR and microarray analyses. ISME J 4:1206–1214. https://doi.org/10.1038/ismej.2010.41.
48. Burkert A, Douglas TA, Waldrop MP, Mackelprang R. 2019. Changes in the active, dead, and dormant microbial community structure across a Pleistocene permafrost chronosequence. Appl Environ Microbiol 85:e02646-18. https://doi.org/10.1128/AEM.02646-18.
49. Hodgkins SB, Chanton JP, Langford LC, McCalley CK, Saleska SR, Rich VI, Crill PM, Cooper WT. 2015. Soil incubations reproduce field methane dynamics in a subarctic wetland. Biogeochemistry 126:241–249. https://doi.org/10.1007/s10533-015-0142-z.
50. Liebner S, Wagner D. 2007. Abundance, distribution and potential activity of methane oxidizing bacteria in permafrost soils from the Lena Delta, Siberia. Environ Microbiol 9:107–117. https://doi.org/10.1111/j.1462-2920.2006.01120.x.
51. Tripathi BM, Kim M, Kim Y, Byun E, Yang J-W, Ahn J, Lee YK. 2018. Variations in bacterial and archaeal communities along depth profiles of Alaskan soil cores. Sci Rep 8:504–511. https://doi.org/10.1038/s41598-017-18777-x.
52. Wagner D, Gattinger A, Embacher A, Pfeiffer E-M, Schloter M, Lipski A. 2007. Methanogenic activity and biomass in Holocene permafrost deposits of the Lena Delta, Siberian Arctic and its implication for the global methane budget. Global Change Biol 13:1089–1099. https://doi.org/10.1111/j.1365-2486.2007.01331.x.
53. Waldrop MP, Wickland KP, White R, III, Berhe AA, Harden JW, Romanovsky VE. 2010. Molecular investigations into a globally important carbon pool: permafrost-protected carbon in Alaskan soils. Glob Chang Biol 16:2543–2554. https://doi.org/10.1111/j.1365-2486.2009.02141.x.
54. Moni C, Lerch TZ, Knoth de Zarruk K, Strand LT, Forte C, Certini G, Rasse DP. 2015. Temperature response of soil organic matter mineralisation in arctic soil profiles. Soil Biol Biochem 88:236–246. https://doi.org/10.1016/j.soilbio.2015.05.024.
55. Gee GW, Or D. 2002. Particle-size analysis. *In* Dane JH, Topp GC (ed), Methods of soil analysis part 4: physical methods. Soil Science Society of America, Inc., Madison, WI.
56. Parada AE, Needham DM, Fuhrman JA. 2016. Every base matters: assessing small subunit rRNA primers for marine microbiomes with mock communities, time series and global field samples. Environ Microbiol 18:1403–1414. https://doi.org/10.1111/1462-2920.13023.
57. Zeleke J, Lu S-L, Wang J-G, Huang J-X, Li B, Ogram AV, Quan Z-X. 2013. Methyl coenzyme M reductase A (*mcrA*) gene-based investigation of methanogens in the mudflat sediments of Yangtze River Estuary, China. Microb Ecol 66:257–267. https://doi.org/10.1007/s00248-012-0155-2.
58. Morris R, Schauer-Gimenez A, Bhattad U, Kearney C, Struble CA, Zitomer D, Maki JS. 2014. Methyl coenzyme M reductase (*mcrA*) gene abundance correlates with activity measurements of methanogenic H_2/CO_2-enriched anaerobic biomass. Microb Biotechnol 7:77–84. https://doi.org/10.1111/1751-7915.12094.
59. Hales BA, Edwards C, Ritchie DA, Hall G, Pickup RW, Saunders JR. 1996. Isolation and identification of methanogen-specific DNA from blanket bog peat by PCR amplification and sequence analysis. Appl Environ Microbiol 62:668–675. https://doi.org/10.1128/aem.62.2.668-675.1996.
60. Caporaso JG, Kuczynski J, Stombaugh J, Bittinger K, Bushman FD, Costello EK, Fierer N, Peña AG, Goodrich JK, Gordon JI, Huttley GA, Kelley ST, Knights D, Koenig JE, Ley RE, Lozupone CA, McDonald D, Muegge BD,

Pirrung M, Reeder J, Sevinsky JR, Turnbaugh PJ, Walters WA, Widmann J, Yatsunenko T, Zaneveld J, Knight R. 2010. QIIME allows analysis of high-throughput community sequencing data. Nat Methods 7:335–336. https://doi.org/10.1038/nmeth.f.303.
61. Mason OU, Case DH, Naehr TH, Lee RW, Thomas RB, Bailey JV, Orphan VJ. 2015. Comparison of archaeal and bacterial diversity in methane seep carbonate nodules and host sediments, Eel River Basin and Hydrate Ridge, USA. Microb Ecol 70:766–784. https://doi.org/10.1007/s00248-015-0615-6.
62. Edgar RC. 2010. Search and clustering orders of magnitude faster than BLAST. Bioinformatics 26:2460–2461. https://doi.org/10.1093/bioinformatics/btq461.
63. Quast C, Pruesse E, Yilmaz P, Gerken J, Schweer T, Yarza P, Peplies J, Glöckner FO. 2013. The SILVA ribosomal RNA gene database project: improved data processing and web-based tools. Nucleic Acids Res 41:D590–D596. https://doi.org/10.1093/nar/gks1219.
64. Mackelprang R, Saleska SR, Jacobsen CS, Jansson JK, Taş N. 2016. Permafrost meta-omics and climate change. Annu Rev Earth Planet Sci 44:439–462. https://doi.org/10.1146/annurev-earth-060614-105126.
65. Coolen MJL, Orsi WD. 2015. The transcriptional response of microbial communities in thawing Alaskan permafrost soils. Front Microbiol 6:197. https://doi.org/10.3389/fmicb.2015.00197.
66. Crevecoeur S, Vincent WF, Comte J, Matveev A, Lovejoy C. 2017. Diversity and potential activity of methanotrophs in high methane-emitting permafrost thaw ponds. PLoS One 12:e0188223. https://doi.org/10.1371/journal.pone.0188223.
67. Schostag M, Stibal M, Jacobsen CS, Bælum J, Taş N, Elberling B, Jansson JK, Semenchuk P, Priemé A. 2015. Distinct summer and winter bacterial communities in the active layer of Svalbard permafrost revealed by DNA- and RNA-based analyses. Front Microbiol 6:411. https://doi.org/10.3389/fmicb.2015.00399.
68. Earth Resources Observation And Science (EROS) Center. 2017. Global 30 Arc-Second Elevation (GTOPO30). Digital elevation model (DEM). U.S. Geological Survey, Reston, VA.
69. Lehner B, Verdin K, Jarvis A. 2008. New global hydrography derived from spaceborne elevation data. Eos Trans AGU 89:93–94. https://doi.org/10.1029/2008EO100001.